

Catalytic hydrogenation of nitrophenols and nitrotoluenes over a palladium/graphene nanocomposite

Cite this: *Catal. Sci. Technol.*, 2014, 4, 1742

Jingwen Sun,^{ab} Yongsheng Fu,^{*a} Guangyu He,^b Xiaoqiang Sun^{*b} and Xin Wang^{*a}

We report a stable palladium/graphene (Pd/G) nanocomposite with differing Pd content for use in the catalytic hydrogenation of nitrophenols and nitrotoluenes. Various microscopic and spectroscopic techniques were employed to characterize the as-prepared catalysts. Catalytic hydrogenation reactions of nitrophenols were conducted in aqueous solution by adding NaBH₄, while the nitrotoluene hydrogenation was carried out in methanol in the presence of H₂ because of the poor solubility in water. The Pd/G hybrids exhibited much higher activity and higher stability than the commercial Pd/C. Due to the presence of a large excess of NaBH₄ compared to *p*-nitrophenol, the kinetic data can be explained by the assumption of a pseudo-first-order reaction with regard to *p*-nitrophenol. The resulting high catalytic activity can be attributed to the graphene sheets' strong dispersion effect for Pd nanoparticles and good adsorption ability for nitrobenzene derivatives *via* π - π stacking interactions. A plausible mechanism is proposed. Considering inductive and conjugation effects that may affect the reactions, the reactivity of nitrophenols in this study is expected to follow the order *m*-NP > *o*-NP > *p*-NP > 2,4-DNP > 2,4,6-TNP, which is in good agreement with the experimental results.

Received 14th January 2014,
Accepted 3rd February 2014

DOI: 10.1039/c4cy00048j

www.rsc.org/catalysis

Introduction

Aminophenols are extensively used in various industries, such as dyes, pesticides, medicine, surfactants and cosmetic products.¹⁻³ As a prominent example, *p*-aminophenol is the most promising intermediate in the industrial synthesis of analgesics and antipyretics, like acetanilide and paracetamol.⁴⁻⁶ It is generally known that nitrophenols are very useful starting materials for producing aminophenols and other chemicals,⁷⁻⁹ though they are considered as one of the top 114 organic pollutants listed by the United State Environmental Protection Agency (USEPA).¹⁰⁻¹² Furthermore, nitrophenols can also be produced as byproducts in industrial processes, for example, the production of nitrobenzene through benzene nitration with nitric and sulfuric acid is usually carried out in continuous mode, forming nitrophenols as the main byproducts, namely, di- and tri-nitrophenols (DNP and TNP).¹³ The multi-nitro compounds are more toxic, carcinogenic, mutagenic, and teratogenic,¹¹⁻¹³ and elimination of these compounds is an

urgent necessity to preserve the environmental quality. Therefore, the development of high performance catalysts for the reduction of nitrophenols to aminophenols is not only valuable for industrial processes, but also very important for the environment.

There are several synthesis routes for the reduction of nitrophenols to aminophenols, including metal/acid reduction, electrolytic reduction and catalytic hydrogenation.^{14,15} It is known that the metal/acid system requires a strong acidic medium and exhibits poor selectivity. The electrolytic reduction needs an acidic or alkaline catholyte, resulting in low yields. Among all the previously mentioned methods, only catalytic hydrogenation is a promising process as it can achieve high conversion, has little impact on the environment and does not generate acid effluents. However, noble metal-based catalysts are still most frequently used in this system, such as palladium,^{16,17} platinum^{18,19} and aurum-based systems,²⁰ which may lead to several unfavorable points such as high cost and limited resources of noble metals.

It is well known that a catalyst support can improve specific properties such as mechanical strength, stability, activity and selectivity of catalysts, and especially it can dilute noble metals in a large volume. Widely used supports include silica, alumina,^{9,21} zeolites,²² TiO₂,²³ polymers²⁴ and carbon materials.²⁵⁻²⁷ In the past few decades, carbon nanomaterials, such as carbon nanotubes and carbon nanofibers, have found numerous promising applications in catalytic hydrogenation. Graphene, as a new

^a Key Laboratory of Soft Chemistry and Functional Materials, (Nanjing University of Science and Technology), Ministry of Education, Nanjing, 210094, China. E-mail: wxin48@163.com, fuyongsheng0925@163.com; Fax: +86 25 8431 5054; Tel: +86 25 84305667

^b Jiangsu Province Key Laboratory of Fine Petrochemical Engineering, Changzhou University, Changzhou 213164, China. E-mail: xqsun@cczu.edu.cn

member of the carbon nanomaterials, exhibits many unique properties, such as high surface area, extraordinary electronic transport properties, superior mechanical stiffness and flexibility. These characteristics make graphene highly desirable for application as a 2D support to load a catalyst.

Pd-based catalysts are known to be capable of selectively hydrogenating nitro-compounds to their corresponding aniline. The combination of graphene sheets and Pd nanoparticles may provide a brand new avenue in utilizing the two-dimensional planar carbon material since it can not only serve as an effective platform for fast transportation of reactants to the catalyst layers, but also result in improved effects of the individual components. Recently, Pd-graphene nanohybrids have been reported to act as catalysts for the Suzuki-Miyaura cross-coupling reactions.²⁸

We have developed a soft chemistry method to directly fabricate metal-graphene nanocomposites, which have been used as catalysts for formic acid and methanol oxidation.^{19,29,30} Since Pd-based catalysts can be used as catalysts for reduction reactions as well, in this study, a Pd/graphene nanocomposite was prepared and used for the hydrogenation of nitrophenols and nitrotoluenes. Herein, we report a stable palladium/graphene nanocomposite for use in the catalytic hydrogenation of nitrophenols and nitrotoluenes. It was found that the π - π stacking interactions are the dominant driving force for the binding between the nitrophenol derivatives and reduced graphene oxide sheets, leading to enhanced adsorption ability of graphene, which helps in promoting the reduction reaction as the reactants can easily gain access to the Pd nanoparticles. The negatively charged hydrogen in the Pd-hydrogen structure can readily attack the positively charged nitrogen in the nitro group. The reactivity of nitrophenols follows the order m -NP > o -NP > p -NP > 2,4-DNP > 2,4,6-TNP.

Experimental

Synthesis of Pd/graphene catalyst

Graphite oxide (GO) was synthesized directly from graphite powder according to the Hummers method.³¹ Palladium/graphene (Pd/G) hybrids with differing Pd contents (5, 10, 20 wt%) were prepared through a hydrothermal method. In a typical procedure, 80 mg of GO was dispersed in a mixture of ethyleneglycol (40 mL) and aqueous solution (20 mL) under ultrasound irradiation for 1 h. Then 40 μ L of Pd(NO₃)₂ was added to the above GO dispersion with magnetic stirring at room temperature for 30 min. The resulting mixture was transferred into a 100 mL Teflon-lined stainless steel autoclave and sealed tightly. The autoclave was then heated to 120 °C and kept there for 12 h. After the solvothermal treatment, the reaction was quenched and cooled to room temperature. The product, denoted as Pd_{0.05}/G, was centrifuged, washed, and finally vacuum freeze-dried overnight. For comparison, 10 wt% and 20 wt% Pd supported on graphene were also prepared under the same experimental conditions, and denoted as Pd_{0.10}/G and Pd_{0.20}/G, respectively.

Characterization

Transmission electron microscopy (TEM) images were taken using a JEOL JEM-2100 microscope operating at 200 kV, by depositing a drop of dispersed sample onto a 300 mesh Cu grid coated with a carbon layer. Powder X-ray diffraction (XRD) analyses were performed on a Bruker D8 Advanced diffractometer with Cu K α radiation and the scanning angle ranged from 5° to 70° of 2θ . Raman spectra of the samples were collected with a Renishaw Reflex Raman Microprobe. X-ray photoelectron spectroscopy (XPS) measurements were carried out on an RBD upgraded PHI-5000C ESCA system (Perkin Elmer) with Mg K α radiation ($h\nu = 1253.6$ eV).

Catalytic hydrogenation of nitrophenols and nitrotoluenes

Catalytic hydrogenation reactions of nitrophenols were conducted at room temperature (25 °C) in the presence of Pd/G catalysts with differing Pd contents. Typically, aqueous solutions of p -nitrophenol (0.3 mM) and NaBH₄ (0.1 M) were freshly prepared. 4 mg of Pd_{0.05}/G was dispersed in 40 mL of p -nitrophenol (p -NP) solution under ultrasound irradiation for several minutes, and then 3 mL of NaBH₄ solution was injected into the mixture under continuous stirring. To evaluate the reaction progress, 3 mL aliquots were taken out of the reaction mixture at specified time intervals and monitored by UV-vis spectroscopy (SHIMADZU TCC-240A). After the reaction, the catalysts can be easily recovered by filtration, and can be reused five times in succession without any treatment. The Pd_{0.10}/G and Pd_{0.20}/G nanocomposites and the commercial Pd/C (5 wt% Sigma-Aldrich 205699) also participated in the hydrogenation, respectively. In addition, the hydrogenation of o -nitrophenol (o -NP), m -nitrophenol (m -NP), 2,4-dinitrophenol (2,4-DNP) and 2,4,6-trinitrophenol (2,4,6-TNP) were carried out under the same conditions.

Unlike for the nitrophenols, the nitrotoluene hydrogenation was carried out in methanol in the presence of H₂ because of the poor solubility in water. The HPLC analyses of the reaction products were performed on a SHIMADZU LC-20A.

Results and discussion

Structure and morphology of Pd/graphene nanocomposite catalyst

Fig. 1a & b show the typical TEM images of the commercial Pd_{0.05}/C and the Pd_{0.05}/G catalysts. It can be seen that there is a more uniform dispersion of Pd nanoparticles on the graphene sheets than on the commercial carbon, thus Pd_{0.05}/G is expected to exhibit a higher efficiency for the catalytic hydrogenation of nitrophenols and nitrotoluenes. The lattice spacing was measured to be 0.223 nm (Fig. 1c), implying that the growth of the Pd nanoparticles occurred preferentially on the (111) planes³² and the average diameter of Pd is about 6.6 nm (Fig. 1d). With increasing loading content, the Pd nanoparticles tend to aggregate as shown in Fig. 1e & f and the aggregation of Pd nanoparticles may be a fatal factor leading to a decrease in catalytic activity.

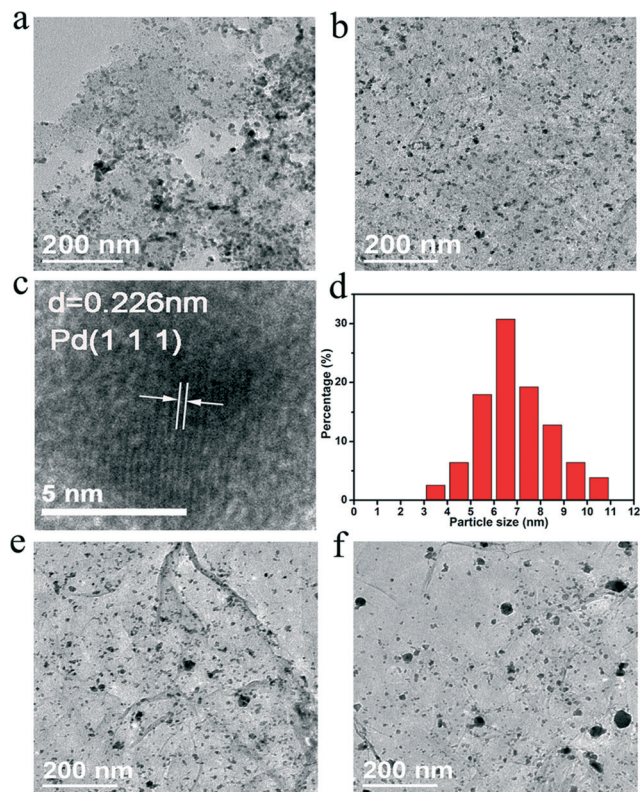


Fig. 1 (a,b) Typical TEM images of the Pd_{0.05}/C and Pd_{0.05}/G catalyst, (c) high-resolution TEM image of the Pd_{0.05}/G catalyst, (d) particle size distribution for the Pd_{0.05}/G catalyst and (e,f) typical TEM images of the Pd_{0.10}/G and Pd_{0.20}/G catalysts.

Fig. 2a shows the X-ray diffraction (XRD) patterns of the as-prepared Pd_{0.05}/G nanocomposite, reduced graphene oxide (RGO) and graphite oxide (GO). It is clear that the Pd_{0.05}/G nanocomposite exhibits an XRD pattern with major peaks at 2θ values of 40.02° , 46.59° and 68.08° , which can be indexed to the (111), (200) and (220) planes of the face-centered cubic (fcc) structure of Pd (JCPDS 46-1043), respectively.³³ Meanwhile, no typical diffraction peak belonging to RGO (002) or GO (001) was observed in the Pd_{0.05}/G nanocomposite. The absence of these peaks may be ascribed to the disruption and exfoliation of graphene oxide in the composites during the hydrothermal reaction. In addition, the average size of Pd

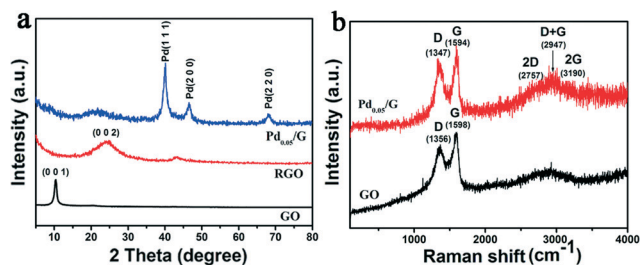


Fig. 2 (a) XRD patterns of Pd_{0.05}/G, RGO and GO, (b) Raman spectra of Pd_{0.05}/G and GO.

particles of the hybrid can be calculated from the (220) peak by the Scherrer equation:³⁴

$$d = \frac{0.9\lambda}{\beta_{1/2} \cos \theta} \quad (1)$$

where d is the average particle size (nm), λ is the wavelength of the X-ray used (0.15406 nm), $\beta_{1/2}$ is the width of the diffraction peak at half height in radians and θ is the angle at the position of the peak maximum. The calculated average particle size of Pd supported on graphene is 5.8 nm, which is consistent with the TEM results.

Raman spectroscopy has been widely used as a powerful tool for characterizing the defect quantity in graphitic materials. Fig. 2b shows the Raman spectra of Pd/G and GO. The D- and G-bands were witnessed at approximately 1359 and 1595 cm^{-1} , which may be assigned to the breathing modes of the κ -point phonons of A_{1g} symmetry and the E_{2g} phonons of sp^2 carbon atoms, respectively.³⁵ Compared to the spectrum of GO, significant peak shifts of the D- and G-bands of Pd/G were observed from 1356 to 1347 cm^{-1} and 1598 to 1594 cm^{-1} , respectively, indicating that GO has been reduced.³⁶ Meanwhile, an increasing D/G intensity ratio was perceived, which is attributed to a lower degree of crystallinity in graphitic materials. Further, the 2D band (2757 cm^{-1}) and combination bands (D + G) were also detected, further indicating the reduction of GO.

X-ray photoelectron spectroscopy (XPS) is the most widely used technique to reveal information about the surface elemental composition and their oxidation states for composites due to its relative simplicity in use and data interpretation. The C 1s core-level spectra of GO and Pd_{0.05}/G are depicted in Fig. 3a & b, respectively. For graphite oxide, the peak at 284.5 eV is associated with C–C bonds, while the interlaced peak centered at the binding energies of 286.1, 287.7 and

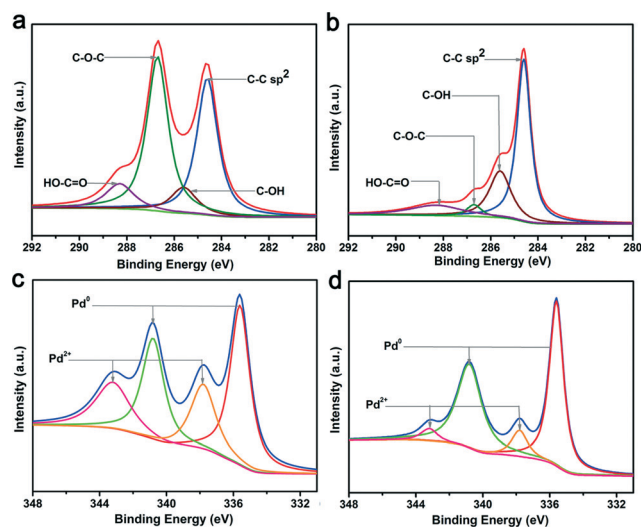


Fig. 3 (a,b) C 1s core-level XPS spectra of GO and the Pd_{0.05}/G catalyst, (c,d) Pd 3d core-level XPS spectrum of commercial Pd_{0.05}/C and the prepared Pd_{0.05}/G catalyst.

289.1 eV can be attributed to the C–OH, C–O–C and OH–C=O functional groups, respectively.³⁷ For Pd_{0.05}/G, the intensity of oxygen-containing groups was obviously reduced during the solvothermal reaction, while the peak at 284.5 eV, corresponding to the C–C bond, became predominant. The splitting pattern of the Pd 3d band of commercial Pd_{0.05}/C and Pd_{0.05}/G consist of two doublets (Fig. 3c & d): the intensive doublet (335.6 and 340.8 eV) may be assigned to metallic Pd and the other doublet (337.8 and 343.2 eV) belongs to the +2 oxidation state of Pd.³⁸ The existence of Pd²⁺ in the catalyst may be due to the reduction of Pd²⁺ not being entirely completed during the solvothermal reaction in the presence of ethylene glycol and the naked metal Pd atoms can be easily oxidized to the form of Pd oxide under ambient conditions.^{39,40} The XPS results also allow us to determine the percentage of the respective oxidation states: 79.7% as Pd(0) and 20.3% as Pd(+2) in Pd/G, while only 60.9% as Pd(0) in Pd/C. The higher the reduction degree of Pd, the higher the catalytic activity for the hydrogenation of nitrophenols.

Catalytic hydrogenation of nitrophenols

The catalytic reduction of *p*-NP by NaBH₄ was chosen as a model reaction to evaluate the catalytic activities of the Pd/G (5, 10 and 20 wt%) catalysts and commercial Pd/C. UV-vis absorption spectra were recorded over time to monitor the change in raw material concentration after adsorption equilibrium. As shown in Fig. 4a, the original adsorption peak of *p*-NP was centered at 317 nm and shifted to 400 nm after the addition of freshly prepared NaBH₄ aqueous solution, and the colour of the solution changed from light yellow to bright yellow immediately. This red shift was just due to the formation of *p*-nitrophenolate ions in alkaline conditions caused by the addition of NaBH₄.¹⁷ After the addition of the Pd_{0.05}/G catalyst,

the peak at 400 nm sharply decreased and a typical absorption of *p*-aminophenol (*p*-AP) at 300 nm increased significantly, and as a result, the initially light yellow solution consequently underwent fading to become colourless.^{39,41}

Fig. 4b shows the absorbance *versus* wavelength plots at various times for the reduction reaction of *p*-NP to *p*-AP in the presence of Pd_{0.05}/G. Fig. 4c shows the relationship of *C/C*₀ *versus* reaction time during the course of the reduction of *p*-NP in the presence of various catalysts, where *C* and *C*₀ are the *p*-NP concentrations at times *t* and 0, respectively. It can be seen that the catalytic activities are in the following order: Pd_{0.05}/G > Pd_{0.10}/G > Pd_{0.05}/C > Pd_{0.20}/G. It should be noted that the activity decreases with increasing Pd content in the catalyst. As shown in Fig. 1e & f, the aggregation of Pd nanoparticles occurred for Pd_{0.10}/G and Pd_{0.20}/G. High Pd loading may result not only in high costs for preparation of catalysts, but also in the increase in particle size due to particle aggregation, leading to lower catalytic activities. As shown in Fig. 4d, the catalyst can be easily separated by a simple centrifugation technique facilitating catalyst recovery and reuse, and the conversion rate of *p*-NP can be maintained at over 85% after five cycles, exhibiting higher activity and higher stability than the commercial Pd/C with the same Pd content.

Since the initial concentration of NaBH₄ largely exceeds that of *p*-NP (~100 times) and the rate of reduction is independent of the concentration of NaBH₄. Thus the reduction rate can be assumed to be independent of NaBH₄ and the hydrogenation process can be described with pseudo-first-order kinetics⁴⁰ with respect to the concentration of *p*-NP:

$$-\ln \frac{C}{C_0} = kt \quad (2)$$

where *C*₀ and *C* (mM) are the concentrations of *p*-NP at beginning and at time *t*, respectively. As shown in Fig. 5, a linear relationship of ln(*C/C*₀) *versus* time was obtained, indicating that the reaction followed pseudo-first-order kinetics. The observed rate constants for Pd_{0.05}/G, Pd_{0.10}/G, Pd_{0.20}/G and Pd_{0.05}/C were 0.0365 s⁻¹, 0.0196 s⁻¹, 0.0024 s⁻¹ and 0.0155 s⁻¹, respectively.

On the basis of the above observations, we propose a plausible mechanism of the catalytic reduction of *p*-NP in the

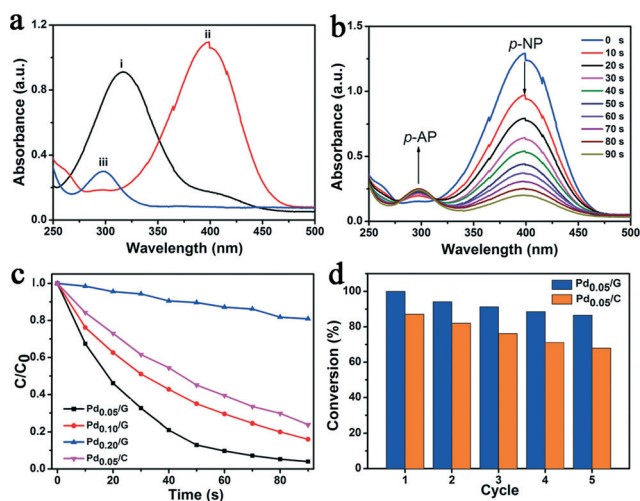


Fig. 4 (a) UV-vis absorption spectra of *p*-NP before (i) and after (ii) the addition of NaBH₄, and *p*-AP (iii), (b) representative time-dependent UV-vis absorption spectra of the reduction of *p*-NP over the Pd_{0.05}/G catalyst in aqueous media at room temperature, (c) hydrogenation of *p*-NP over different catalysts, (d) reuse of Pd_{0.05}/G and Pd_{0.05}/C catalysts for *p*-NP reduction.

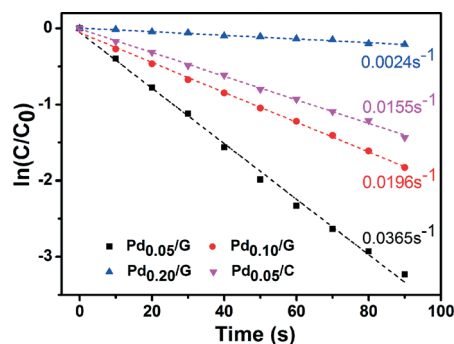


Fig. 5 Plot of ln(*C/C*₀) against reaction time for the catalytic reduction of *p*-NP with different catalysts.



Scheme 1 A plausible mechanism for the reduction of *p*-nitrophenol catalyzed by the Pd/G catalyst in the presence of sodium borohydride.

presence of NaBH_4 as shown in Scheme 1. In the reaction system, the π - π stacking interactions are the dominant driving force for the binding between the nitrophenols and reduced graphene oxide sheets, leading to enhanced adsorption abilities of graphene.^{42,43} Good adsorption helps in promoting the reduction reaction as the nitrophenol molecules can easily gain access to the Pd nanoparticles.⁴⁴ NaBH_4 can react with water at ambient temperature, yielding H_2 and the sodium metaborate (NaBO_2) by-product. In the presence of Pd nanoparticles, the H-H bond in H_2 cleaves, and each hydrogen attaches to the metal nanoparticle surface, forming metal-hydrogen bonds. The negatively charged hydrogen in the metal-hydrogen structure can easily attack the positively charged nitrogen in the nitro group of nitrophenols, and as a result, the nitro group is reduced to the nitroso group, followed by the reductive addition of two hydrogen atoms to form hydroxylamine. Finally, the hydroxylamine is further reduced to the aniline derivative.

Catalytic hydrogenation of more nitrophenols, such as *o*-NP, *m*-NP, 2,4-DNP and 2,4,6-TNP, was also conducted with freshly prepared NaBH_4 in the presence of $\text{Pd}_{0.05}/\text{G}$, and the results are shown in Fig. 6.

Because of the conjugation effect of *o*-NP and *p*-NP, the negative charge in the phenoxide ion may be delocalized onto the nitro group, making the group more stable. Moreover, the inductive effect may also play a certain role, which is dependent on the distance between the substituent group and the group that reacts, so that the inductive effect of *o*-NP is stronger than that of *p*-NP. The stronger inductive

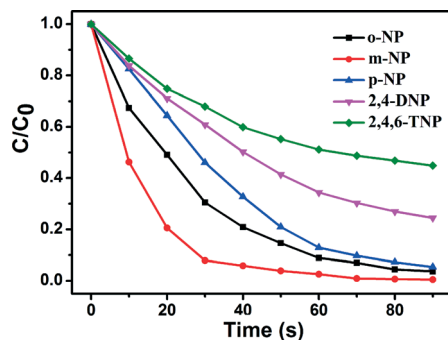


Fig. 6 Plot of C/C_0 versus time during the course of reduction of various nitrophenols with $\text{Pd}_{0.05}/\text{G}$.

Table 1 Pseudo-first-order kinetics study with nitrophenols and different catalysts

Catalyst	Raw material	k (min^{-1})	Catalyst	Raw material	k (min^{-1})
$\text{Pd}_{0.05}/\text{G}$	<i>p</i> -NP	2.192	$\text{Pd}_{0.05}/\text{G}$	<i>o</i> -NP	2.279
$\text{Pd}_{0.10}/\text{G}$		1.176	$\text{Pd}_{0.05}/\text{G}$	<i>m</i> -NP	3.562
$\text{Pd}_{0.20}/\text{G}$		0.144	$\text{Pd}_{0.05}/\text{G}$	<i>p</i> -NP	2.192
$\text{Pd}_{0.05}/\text{C}$		0.932	$\text{Pd}_{0.05}/\text{G}$	2,4-DNP	0.974
			$\text{Pd}_{0.05}/\text{G}$	2,4,6-TNP	0.531

effect of *o*-NP makes its nitrogen atom more positively charged, resulting in higher reactivity. For *m*-NP, the phenoxide oxygen is not directly conjugated to the *meta*-nitro group and thus the inductive effect alone stabilizes the nitro group to a smaller extent. Taking into account the structure of nitrophenols with mono- and multi-nitro groups, mono-nitrophenol has the smallest steric resistance and 2,4,6-TNP has the largest one. Based on the discussion above, the reactivity of nitrophenols in this study is expected to follow the order $m\text{-NP} > o\text{-NP} > p\text{-NP} > 2,4\text{-DNP} > 2,4,6\text{-TNP}$, which is in good agreement with the experimental results (Table 1).

Influence of substitution at phenyl positions on hydrogenation reactions

Nitrophenols and nitrotoluenes were selected as models to evaluate the comparative influence of substitution at different phenyl positions on the hydrogenation reactions. Because of the poor solubility of nitrotoluenes in water, the solvent and reducing agent were replaced by methylalcohol and hydrogen, respectively. The hydrogenation conversion rates of nitrobenzenes substituted by $-\text{OH}$ or $-\text{CH}_3$ at different positions (*ortho*-, *meta*- or *para*-) were calculated and summarized in Table 2, where it can be found that the conversion rate of nitrotoluene was nearly three times as much as that of

Table 2 Reduction of nitrophenols and nitrotoluenes with hydrogen in the presence of methylalcohol

Catalyst	R	Product	Conversion (%)
$\text{Pd}_{0.05}/\text{G}$	$-\text{OH}$		35.72
			40.82
			29.55
	$-\text{CH}_3$		89.32
			100.0
			80.33

nitrophenol substituted at the same site. This phenomenon can be attributed to the electron donating ability of the methyl group being weaker than that of the hydroxyl group, and as a result, the more positively charged nitrogen can be more easily attached to the negatively charged hydrogen from the Pd metal-hydrogen structure. Similar to nitrophenols, for *o*-nitrotoluene or *p*-nitrotoluene, the negative charge in the toluene-ring may be delocalized into the nitro group, making the group more stable. Further considering that the inductive effect of *o*-nitrotoluene is stronger than that of *p*-nitrotoluene, the former is expected to exhibit higher reactivity. For *m*-nitrotoluene, the toluene-ring is not directly conjugated to the *meta*-nitro group and thus the inductive effect alone stabilizes the nitro group to a smaller extent. Thus, the reactivity of nitrotoluenes in this study follows the order *m*-nitrotoluene > *o*-nitrotoluene > *p*-nitrotoluene, which is consistent with the experimental results.

Conclusions

In summary, we have fabricated and characterized a stable palladium/graphene nanocomposite with differing Pd content for use in the catalytic hydrogenation of nitrophenols and nitrotoluenes. Catalytic hydrogenation reactions of nitrophenols were carried out in an aqueous solution by adding NaBH₄, the Pd/G hybrids exhibited much higher activity and higher stability than the commercial Pd/C. It was found that the π - π stacking interactions may enhance adsorption ability of graphene, which helps in promoting the reduction reaction as the reactants can easily gain access to the surface of the Pd particles. Taking into account the inductive and conjugation effects, the reactivity of nitrophenols may follow the order *m*-NP > *o*-NP > *p*-NP > 2,4-DNP > 2,4,6-TNP, which is consistent with the experimental results. Because of the poor solubility of nitrotoluenes in water, the hydrogenation was conducted in methanol in the presence of H₂. The reactivity of nitrotoluenes was found to be *m*-nitrotoluene > *o*-nitrotoluene > *p*-nitrotoluene.

Acknowledgements

This investigation was supported by NNSF of China (no. 21171094), NSAF (no. U1230125), RFDP (no. 20123219130003), STPP of Jiangsu (no. BE 2012151), the Fundamental Research Funds for the Central Universities (no. 30920130122002), PAPD of Jiangsu and the Jiangsu Province Key Laboratory of Fine Petrochemical Engineering (no. KF1206).

Notes and references

- 1 T. Joseph, K.-V. Kumar, A.-V. Ramaswamy and S.-B. Halligudi, *Catal. Commun.*, 2007, **8**, 629.
- 2 J.-M. Zhang, G.-Z. Chen, M. Chaker, F. Rosei and D.-L. Ma, *Appl. Catal., B*, 2013, **132–133**, 107.
- 3 S. Gazi and R. Ananthkrishnan, *Appl. Catal., B*, 2011, **105**, 317.
- 4 N. Sahiner, H. Ozay, O. Ozay and N. Aktas, *Appl. Catal., B*, 2010, **101**, 137.
- 5 I.-H.-A.-E. Maksod, E.-Z. Kenawy and T.-S. Saleh, *Adv. Synth. Catal.*, 2010, **352**, 1169.
- 6 J. Li, C.-Y. Liu and Y. Liu, *J. Mater. Chem.*, 2012, **22**, 8426.
- 7 Q. An, M. Yu, Y.-T. Zhang, W.-F. Ma, J. Guo and C.-C. Wang, *J. Phys. Chem. C*, 2012, **116**, 22432.
- 8 D. Aktas and F. Cecen, *J. Hazard. Mater.*, 2010, **177**, 956.
- 9 A.-Y. Atta, B.-Y. Jibril, T.-K. Al-Waheibi and Y.-M. Al-Waheibi, *Catal. Commun.*, 2012, **26**, 112.
- 10 J.-W. Zhang, C.-P. Hou, H. Huang, L. Zhang, Z.-Y. Jiang, G.-X. Chen, Y.-Y. Jia, Q. Kuang, Z.-X. Xie and L.-X. Zheng, *Small*, 2013, **9**, 538.
- 11 D. Sreekanth, D. Sivaramkrishna, V. Himabindu and Y. Anjaneyulu, *J. Hazard. Mater.*, 2009, **164**, 1532.
- 12 J. Feng, L. Su, Y.-H. Ma, C.-L. Ren, Q. Guo and X.-G. Chen, *Chem. Eng. J.*, 2013, **221**, 16.
- 13 M.-K.-K. Oo, C.-F. Chang, Y.-Z. Sun and X.-D. Fan, *Analyst*, 2011, **136**, 2811.
- 14 F.-D. Popp and H.-P. Schultz, *Chem. Rev.*, 1962, **62**, 19.
- 15 I.-H.-A.-E. Maksod and T.-S. Saleh, *Green Chem.*, 2010, **3**, 127.
- 16 C. Jouannin, I. Dez, A.-C. Gaumont, J.-M. Taulemesse, T. Vincentand and E. Guibal, *Appl. Catal., B*, 2011, **103**, 444.
- 17 A.-R. Siamaki, A.-E.-R.-S. Khder, V. Abdelsayed, M.-S. El-Shall and B.-F. Gupton, *J. Catal.*, 2011, **279**, 1.
- 18 M.-H. Liu, J. Zhang, J.-Q. Liu and W.-W. Yu, *J. Catal.*, 2011, **278**, 1.
- 19 H.-J. Huang, H.-Q. Chen, D.-P. Sun and X. Wang, *J. Power Sources*, 2012, **204**, 46.
- 20 P. Dauthal and M. Mukhopadhyay, *Ind. Eng. Chem. Res.*, 2012, **51**, 13014.
- 21 F. Cárdenas-Lizana, S. Gomez-Quero and M.-A. Keane, *Chem. Commun.*, 2008, 475.
- 22 J. Horáček, G. St'ávoová, V. Kelbichová and D. Kubicka, *Catal. Today*, 2013, **204**, 38.
- 23 A. Yoshida, Y. Mori, T. Ikeda, K. Azemoto and S. Naito, *Catal. Today*, 2013, **203**, 153.
- 24 C.-H. Yuan, Y.-T. Xu, W.-A. Luo, B.-R. Zeng, W.-H. Qiu, J. Liu and H.-L. Huang, *Nanotechnology*, 2012, **23**, 175301.
- 25 Q.-F. Shi and G.-W. Diao, *Electrochim. Acta*, 2011, **58**, 399.
- 26 Y.-X. Sua, B.-X. Fan, L.-S. Wang, Y.-F. Liu, B.-C. Huang, M.-L. Fu, L.-M. Chen and D.-Q. Ye, *Catal. Today*, 2013, **201**, 115.
- 27 I.-C.-M.-J. López, S. Fraile and J.-A. Alonso, *J. Phys. Chem. C*, 2012, **116**, 21179.
- 28 G.-M. Scheuermann, L.-G. Rumi, P. Steurer, W. Bannwarth and R. Mulhaupt, *J. Am. Chem. Soc.*, 2009, **131**, 8262.
- 29 H.-J. Huang and X. Wang, *J. Mater. Chem.*, 2012, **22**, 22533.
- 30 C. Xu, X. Wang and J.-W. Zhu, *J. Phys. Chem. C*, 2008, **112**, 19841.
- 31 W.-S. Hummers and R.-E. Offeman, *J. Am. Chem. Soc.*, 1958, **80**, 1339.
- 32 F. Peirano, T. Vincent, F. Quignard, M. Robitzer and E. Guibal, *J. Membr. Sci.*, 2009, **329**, 30.
- 33 G.-H. Jeong, S.-H. Kim, M. Kim, D. Choi, J.-Y. Lee, J. Kim and S. Kim, *Chem. Commun.*, 2011, **47**, 12236.
- 34 H.-J. Huang, Y. Fan and X. Wang, *Electrochim. Acta*, 2012, **80**, 118.
- 35 Y.-J. Li, W. Gao, L.-J. Ci, C.-M. Wang and P.-M. Ajayan, *Carbon*, 2010, **48**, 1124.

- 36 T.-N. Lambert, C.-A. Chavez, B. Hernandez-Sanchez, P. Lu, N.-S. Bell, A. Ambrosini, T. Friedman, T.-J. Boyle, D.-R. Wheeler and D.-L. Huber, *J. Phys. Chem. C*, 2009, **113**, 19812.
- 37 A. Halder, S. Sharma, M.-S. Hegde and N. Ravishankar, *J. Phys. Chem. C*, 2009, **113**, 1466.
- 38 H.-J. Huang and X. Wang, *Phys. Chem. Chem. Phys.*, 2013, **15**, 10367.
- 39 M. Ohashi, K.-D. Beard, S. Ma, D.-A. Blom, J. St-Pierre, J.-W.-V. Zee and J.-R. Monnier, *Electrochim. Acta*, 2010, **55**, 7376.
- 40 L. Feng, F. Si, S. Yao, W. Cai, W. Xing and C. Liu, *Catal. Commun.*, 2011, **12**, 772.
- 41 S. Praharaj, S. Nath, S.-K. Ghosh, S. Kundu and T. Pal, *Langmuir*, 2004, **20**, 9889.
- 42 P. Xiong, Q. Chen, M.-Y. He, X.-Q. Sun and X. Wang, *J. Mater. Chem.*, 2012, **22**, 17485.
- 43 G.-H. Zuo, X. Zhou, Q. Huang, H.-P. Fang and R.-H. Zhou, *J. Phys. Chem. C*, 2011, **115**, 23323.
- 44 D. Ravellia, D. Dondib, M. Fagnonia and A. Albini, *Chem. Soc. Rev.*, 2009, **38**, 1999.